MDPI

Review

Development of Bottom-Blowing Copper Smelting Technology: A Review

Baojun Zhao * and Jinfa Liao

Faculty of Materials Metallurgy and Chemistry, Jiangxi University of Science and Technology, Ganzhou 341000, China; liaojinfa678@outlook.com
* Correspondence: bzhao@jxust.edu.cn

Abstract: Bottom-blowing copper smelting technology was initiated and developed in China in the 1990s. Injection of oxygen-enriched high-pressure gas strongly stirs the molten bath consisting of matte and slag. Rapid reaction at relatively lower temperatures and good adaptability of the feed materials are the main advantages of this technology. Development and optimisation of bottom-blowing copper smelting technology were supported by extensive studies on the thermodynamics of the slag and the fluid dynamic of the molten bath. The history of technological development and fundamental studies related to this technology are reviewed in this paper.

Keywords: copper smelting; bottom-blowing; SKS; slag; fluid dynamic

1. Introduction

Smelting is one of the important processes in the pyrometallurgical production of blister copper in which copper–iron sulphides are oxidised to form molten matte and slag. Flash smelting and bath smelting are the major smelting technologies in copper production. Copper concentrates react with oxygen directly in the flash smelting process which has the advantages of high capacity and automatic control. However, fine and dry feeds are required for the flash smelting furnace to enable fast reactions. As a result, considerable feed preparation is required, and the dust rate is relatively higher. It has limited ability to treat scrap and other copper-containing materials with large sizes. Bath smelting is an alternative technology to flash smelting which involves the reactions of copper concentrate with oxygen in the molten bath. Several technologies have been developed based on the bath smelting principles that include IsaSmelt/Ausmelt, Noranda/El Teniente, Vanyukov, Mitsubishi and recently developed bottom-blowing smelting (BBS) process [1–4]. Due to its unique technological features, such as good adaptability to raw materials, high oxygen utilisation and thermal efficiency, and flexible capacity, BBS technology has attracted strong interest from the copper industry [5–14]. In 2016, 13 BBS furnaces were constructed or were under construction with the capacity of 1600 kt/a copper production. The furnace size ranged from Ø3.8 m × 11.5 m to Ø5.8 m × 30 m [5,14]. The fundamental studies including thermodynamics of the slag and fluid dynamic of the molten bath have been extensively conducted in recent years to understand and support the new technology. This review summarises the development of the copper BBS including the history, features and relevant fundamental studies.

2. History of Technology Development

From November 1991 to June 1992, a plant trial was conducted at Shuikoushan (SKS) Smelter for a period of 217 days to smelt copper concentrate in a bottom-blowing furnace [15,16]. The name of SKS Smelting Technology was therefore used initially to represent the bottom-blowing copper smelting technology. Figure 1 below shows the flowsheet of the SKS trial [16]. It can be seen from the figure that carbon fuel was used during the trial, and the feeds were palletised during the trial. The smelting slag was

treated by flotation process to recover copper and the concentrate from the flotation was sent back to the bottom-blowing furnace (BBF). Only the coarse flue dust from the BBF and PS converter was sent back to the BBF. The detailed operating parameters are given in Table 1. It can be seen from Table 1 that the BBF treated 50 t feeds per day during the trial and Cu in the concentrate was approximately 20%. Matte with 50% Cu was produced and Cu in the slag was in the range of 1–3%. Oxygen utilization at 100% was claimed and a lance life of 5000 h was estimated.
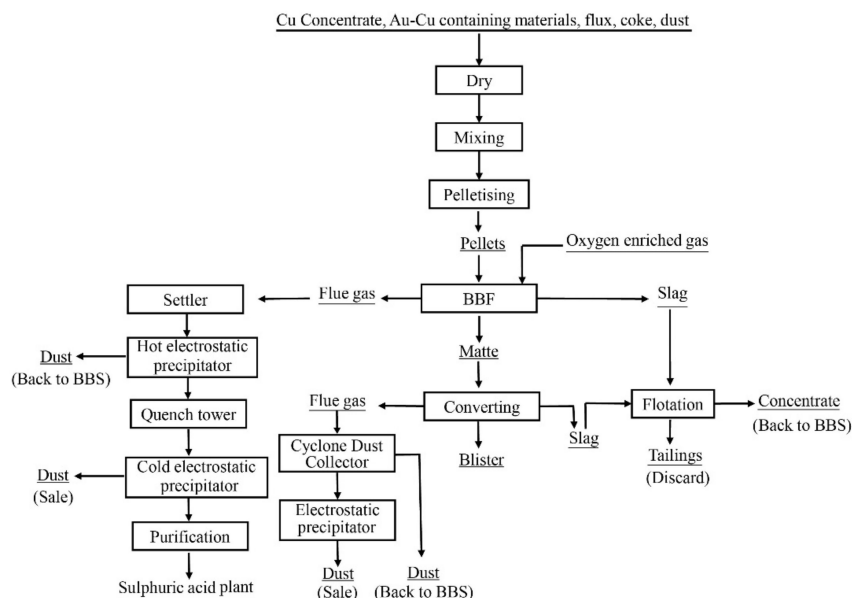

Figure 1. Flowsheet of SKS copper smelting technology, adapted from [16].

Table 1. Detailed operating parameters during SKS trial. Data derived from [16].

Parameter	Unit	SKS
Capacity	t/d	50
Cu in Concentrate	%	~20
Fe in Concentrate	%	~26
S in Concentrate	%	25~30
Matte grade	%	~50
Cu in slag	%	1~3
Slag clean	-	flotation
Cu in tailing	%	0.34
Fe/SiO$_2$ in slag	-	1.5~1.7
O$_2$ in gas	vol%	60~70
Oxygen pressure	Mpa	0.5~0.7
O$_2$ utilisation	%	100
Lance life	hour	5000
Production rate	%	81.4
SO$_2$ in gas	vol%	>20
Cu direct recovery	%	93
Cu total recovery	%	98
Furnace campaign life	day	>330

In 2005 the first industrial scope BBF was built in Sin Quyen smelter in Vietnam. The size of the furnace was Ø3.8 m × 11.5 m and the capacity was designed to be 10,000 t Cu per year [6,17]. However, the BBF in Sin Quyen smelter seemed not operating properly as no operating details were reported. In 2008 the first real commercialised BBF started in Dongying Fangyuan Nonferrous Metals (Fangyuan) [7]. The main equipment was a horizontal cylindrical furnace shown in Figure 2. The size of the furnace was Φ 4.4 m × 16.5 m and it was lined with 380 mm thick chrome-magnesia bricks. The BBF had nine gas lances arranged in two rows on the bottom, five lances at 7 degrees and four lances at 22 degrees towards the outside. Each lance consisted of an inside tube and an external shroud. The inside tube injected pure oxygen and the shroud injected airflow as a coolant to protect the lance. The furnace operated with a rotation mechanism so the lances could be rolled above the molten bath during maintenance, repair, power failure or another emergency. Mixed feed materials with 7–10 wt% moisture were continuously transported by a belt conveyor into the high-temperature melt in the furnace through a feed mouth located above the reaction zone. High-pressure oxygen and air were blown constantly by the lances into the copper matte, in which iron and sulphur were rapidly oxidised. The by-product SO_2 was sent to the acid plant and the slag was tapped regularly followed by the flotation process to recover copper. Matte was tapped regularly and sent to the PS converters by a ladle.
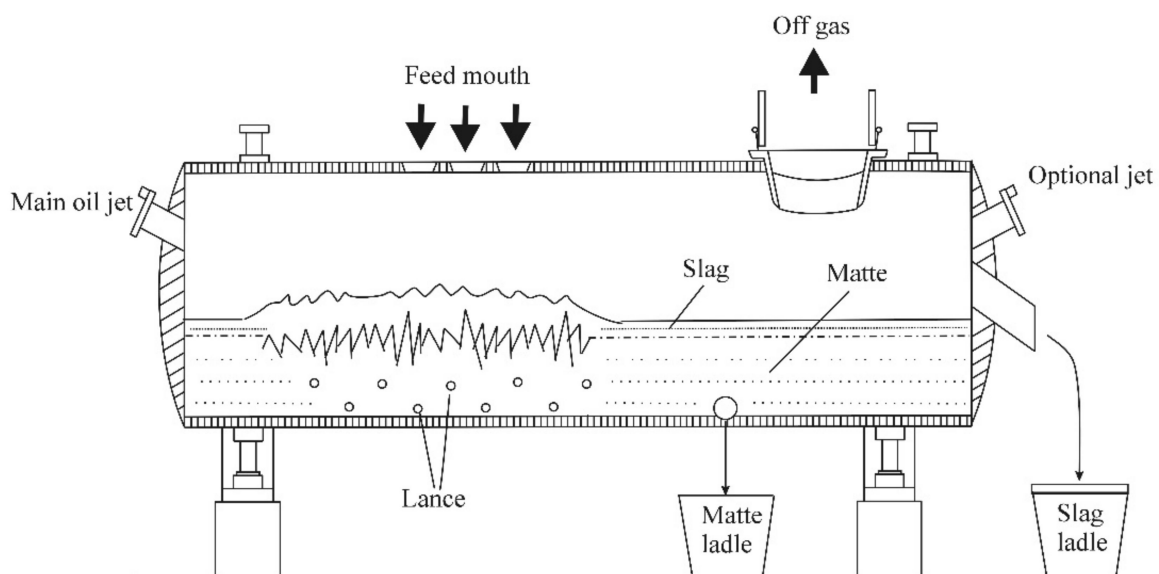

Figure 2. The bottom-blowing furnace at Dongying Fangyuan Nonferrous Metals. Reprinted with permission from ref. [7]. Copyright 2021 John Wiley and Sons.

Table 2 shows key process parameters in the Fangyuan smelting plant in January 2012 compared with the initial design. The effort made by the management and engineers enabled unexpected performance to be achieved in the first commercialised BBF. Differently from the trials in Shuikoushan, the following advantages were demonstrated in the Fangyuan BBF:

(1).   No carbon fuel was used—no CO_2 was generated.
(2).   Feed preparation was not required—up to 100 mm size could be fed into the BBF directly.
(3).   High-grade matte with 70% Cu was produced—more concentrate could be treated.
(4).   Concentrate feed rate increased from 32 to 75 dry t/h—the furnace capacity was more than doubled.

Table 2. Typical process parameters for Fangyuan smelting plant in January 2012. Data derived from [7].

Parameter	Unit	Design	January 2012
Maximum concentrate feed rate	dry t/h	32	75
Average concentrate feed rate	dry t/h	32	70
Average Cu content in concentrate	%	25	22
Average moisture of the feed	%	8	7
Average silica flux feed rate	dry t/h	-	8
Average coal feed rate	dry t/h	2.46	0–0.8
Total average feed to the furnace	wet t/h	-	90
Average copper matte grade	%	55	70
Average Fe/SiO_2 in slag	-	1.7	1.8
Average Cu in smelting slag	%	4	2.6
Average Cu in flotation tailing slag	%	0.42	0.3
Average oxygen + air flow rate	Nm^3/s	-	4.2
Average oxygen enrichment	%	70	72
Bath temperature range	°C	1180–1200	1150–1170

Compared with other bath smelting technologies, BBF shows several advantages:

(1). Less preparation of feeds

Top blowing technology (Ausmelt and Isasmelt) requires pelletised feeds and side blowing technology (Teniente Converter) needs to inject dry and fine particle feeds. BBF can treat a wide range of size feeds up to 100 mm diameter with moisture up to 10%.

(2). High gas pressure and long lance life

Much higher gas pressure in BBF has many advantages confirmed by Kapusta et al. [18–23]. As one of the significant developments at Fangyuan, a series of trials were undertaken to identify the optimum pressures of the oxygen and air in the lances. It was found that optimum gas pressures were related to the feeding rate, the viscosity of the slag, thicknesses of the slag and matte layers. The following requirements need to be met: (1) no backflow of matte into the lances; (2) enough stirring for rapid reactions and generation of the surface wave; (3) no strong splashing of the slag and matte to block the feed mouth and (4) a protection accretion is formed at the tip of the lance. Figure 3 shows the "mushroom" formed at the tip of the lances which enabled the lance life to be over 10 months [7]. These mushroom tips not only protect the lances but also distribute the injected gases to small bubbles.

(3). Autogenous Smelting

Autogenous operation was achieved in the BBF at Fangyuan for smelting of normal copper concentrates. This operation reduced energy consumption and CO_2 emission. The autogenous smelting was obtained by (1) low-temperature operation; (2) low slag rate resulting in a high Fe/SiO_2 ratio; (3) low off-gas volume resulting in high oxygen concentration; (4) high thermal efficiency as most of the oxidisation reactions occur in the lower part of the bath, the heat generated from these reactions can be efficiently absorbed by the molten matte and slag.

(4). Low-Temperature Smelting

The slag temperatures measured at the taphole of the Fangyuan BBF were usually in the range of 1150 to 1170 °C which was much lower than the liquidus temperature of the slag [7,24]. Approximately 20% solid spinel was present in the slag which increased the slag viscosity significantly. High-pressure gases injected from the bottom of the molten bath can generate surface waves that push the viscous slag out of the furnace through the taphole. The advantages of low-temperature smelting are (1) no extra fuels are required to maintain smelting temperature (although oil jets were available on both ends of the BBF, they were rarely used); (2) low consumption of the refractory. There was no significant erosion of the refractory on most parts of the furnace after one and a half years operation since spinel accretion was formed to protect the refractory [24–27]; (3) relatively higher viscosities of the matte and slag allowed higher pressures of the injected gases without

strong splashing; (4) a higher-grade matte can be produced at a lower temperature at a given oxygen partial pressure.
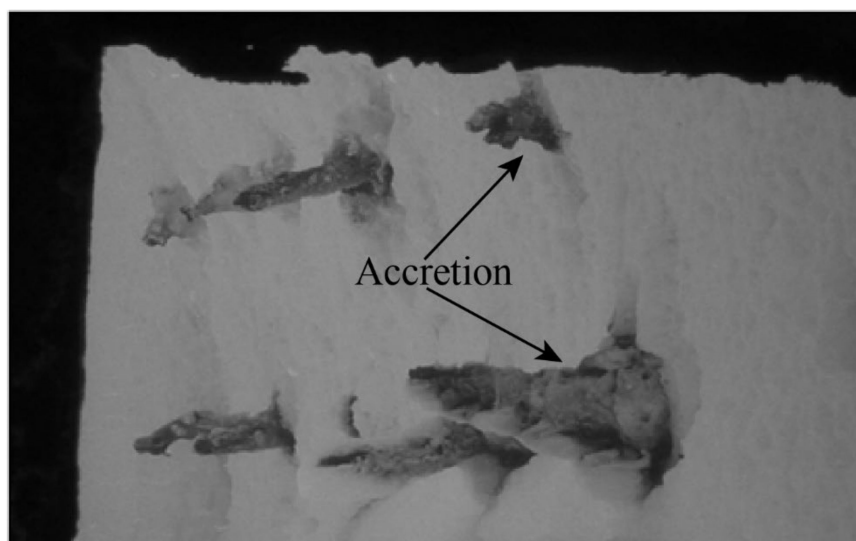

Figure 3. "Mushroom" tips formed on the lances of the Fangyuan BBF. Reprinted with permission from ref. [7]. Copyright 2021 John Wiley and Sons.

3. Fundamental Studies to Support Development of BBS Technology

3.1. Slag Chemistry

In the conventional theory of pyrometallurgy, the slag temperature must be higher than its liquidus temperature to avoid the formation of the solid phase. In Fangyuan BBF operation, high matte grade and high Fe/SiO_2 in the slag resulted in a high liquidus temperature of the smelting slag. In contrast, the BBF slag temperature was lower than other copper smelting technologies [7,28–30]. It was doubted widely that either slag composition or temperature was not reliable. Researchers from the University of Queensland measured the slag tapping temperatures carefully using a K-type thermocouple and collected quenched slag samples. In combination with electron probe X-ray microanalysis (EPMA) and thermodynamic analyses [31], it was confirmed that it is possible to operate BBF with a viscous slag containing solid phase.

Figure 4 shows a typical microstructure of the quenched BBF slag compared with the FSF slag [7]. It can be seen from Figure 4a that liquid, spinel and matte phases were present in the slag. The shape and size of the spinel phase indicate that the spinel was the primary phase presented at high temperatures. The slag tapping temperature of the BBF was therefore lower than its liquidus temperature. The matte droplets in different sizes were also present in the slag. In contrast, it can be seen from Figure 4b that no solid phase was found in the quenched flash smelting slag. The compositions of the phases present in a quenched BBF slag were measured by EPMA and are shown in Table 3 together with the bulk composition measured by XRF. Both EPMA and XRF can only measure elemental compositions. The compositions shown in the table were calculated by assuming that the elements were present in certain forms of oxides or elements in the slag. It is estimated from the compositions that the proportion of the spinel is approximately 16.8 wt%.

Reheating experiments were carried out using the slag shown in Table 3 under ultra-high purity Ar flow. The experiments were undertaken at 1150, 1200, 1250 and 1300 °C respectively using Pt foil. In these experiments, the oxygen partial pressure was not controlled, it was assumed that there was no oxygen exchange between the slag and Ar gas. FactSage was used to simulate the reheating experiments. The experimentally determined proportion of liquid phase from mass balance was compared with FactSage predictions. It can be seen from Figure 5 that both experimental data and FactSage predictions showed the proportion of liquid phase decreased slowly with decreasing temperature between

1150 and 1300 °C [7]. This indicates that equilibrium was obtained during the reheating experiments and the FactSage predictions were relatively reliable under the condition used. Reheating experiments were not undertaken below 1150 °C. It can be seen from the figure that, according to the FactSage predictions, the proportion of liquid phase decreases sharply if the temperature is lower than 1150 °C due to the formation of other solid phases such as olivine and silica.
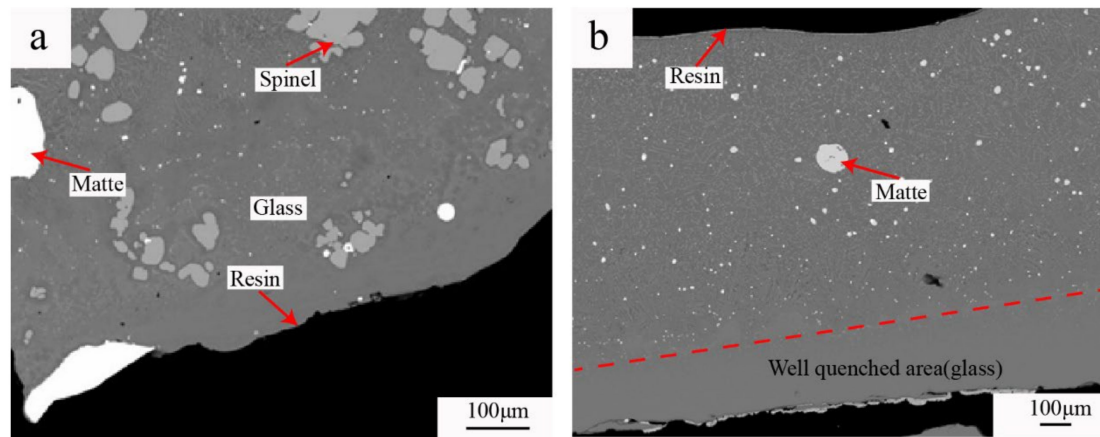

Figure 4. Typical microstructures of quenched smelting slag from Fangyuan BBF (**a**) (Reprinted with permission from ref. [7]. Copyright 2021 John Wiley and Sons) and a flash furnace (**b**).

Table 3. Compositions of the phases present in a quenched BBF slag measured by EPMA and bulk composition measured by XRF (wt%). Data derived from [7].

Phases	FeO	Cu_2O	CaO	SiO_2	Al_2O_3	As_2O_3	MgO	S	PbO	ZnO	MoO_3
bulk-XRF	62.2	3.20	1.00	24.2	3.10	0.100	0.600	1.70	0.500	3.10	0.200
glass	58.4	0.800	1.20	30.5	3.20	0.100	0.700	1.10	0.500	3.30	0.200
spinel	93.7	0.100	0.000	0.600	3.40	0.000	0.300	0.00	0.100	1.70	0.100
matte	10.1	68.9	0.000	0.000	0.00	0.100	0.000	20.3	0.100	0.200	0.300

3.2. Phase Equilibria

It can be seen from Table 3 that significant amounts of Al_2O_3, CaO, MgO and ZnO are present in the BBF slag which can influence the liquidus temperature of the slag. Systematic studies were conducted under controlled oxygen partial pressures to evaluate the effects of these components on liquidus temperature of the copper smelting slag [32–39]. Figure 6 shows liquidus temperature as a function of Fe/SiO_2 weight ratio at $Po_2 = 10^{-8}$ atm [32]. The lines in the figure were calculated by FactSage 6.2 [31] and the symbols represent experimental data. It can be seen that spinel and tridymite are the primary phases in the composition range investigated for "FeO"–SiO_2, "FeO"–SiO_2–CaO and "FeO"–SiO_2–CaO–Al_2O_3 slags. Olivine and wustite primary phase fields replaced spinel primary phase fields when 4 wt% CaO and 4 wt% MgO are present in the slag. Additions of CaO and Al_2O_3 move the low-liquidus region towards a low Fe/SiO_2 direction and increase the liquidus temperatures in the spinel primary phase field. FactSage predictions showed similar trends on the liquidus temperature as the experimental results. However, there are significant differences in liquidus temperatures between FactSage predictions and experimental results in some areas indicating that the FactSage database needs to be improved.
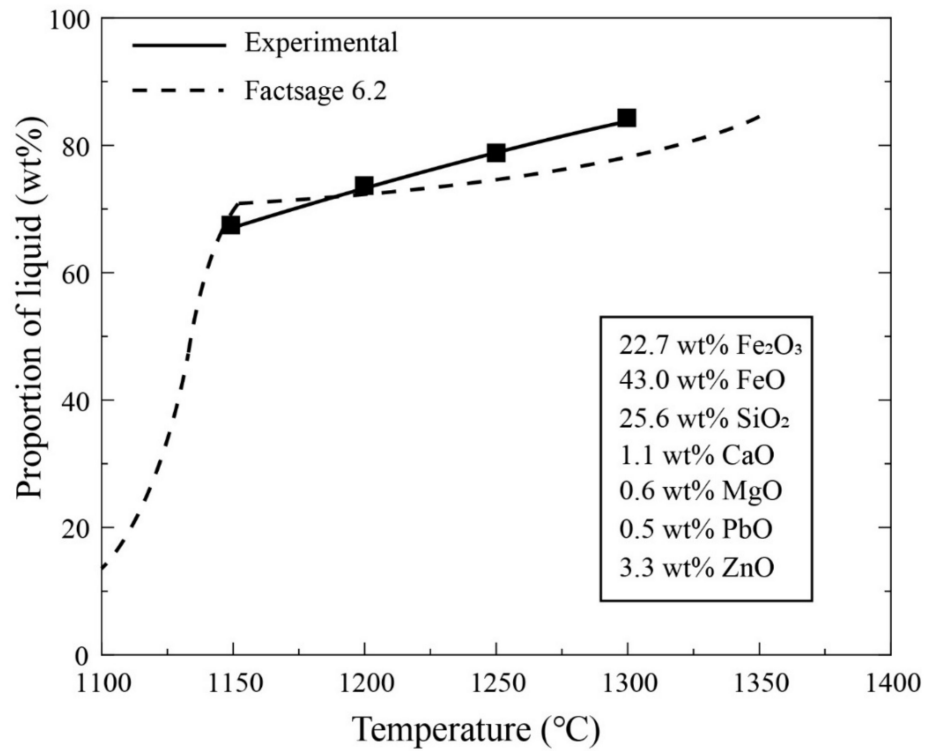
Figure 5. Proportion of liquid as a function of temperature for a typical BBF slag, in comparison between experimental results and FactSage 6.2 predictions. Reprinted with permission from ref. [7]. Copyright 2021 John Wiley and Sons.
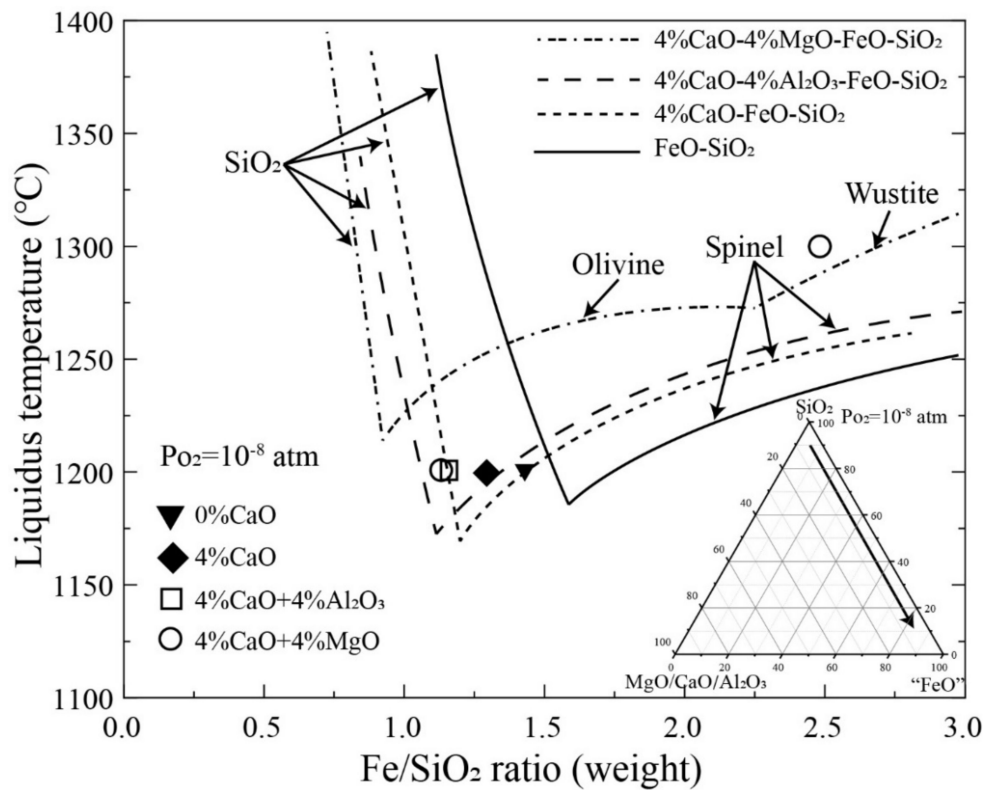

Figure 6. Liquidus temperature as a function of Fe/SiO_2 weight ratio, $Po_2 = 10^{-8}$ atm, lines were calculated by FactSage 6.2, symbols are experimental results in spinel (1200 °C) and wustite (1300 °C) primary phase fields [32].

The phase equilibria in the system ZnO–"FeO"–SiO$_2$–Al$_2$O$_3$–CaO–MgO were systematically studied under controlled oxygen partial pressure by Liu et al. [33–36]. Figure 7 shows the effects of ZnO, Al$_2$O$_3$, CaO and MgO on liquidus temperatures at fixed FeO/SiO$_2$ = 1.9 and Po$_2$ 10^{-8} atm [33]. Spinel is the only primary phase at the given conditions without MgO. Olivine is the primary phase when 4 wt% MgO and less than 2 wt% ZnO are present. It can be seen from the figure that, the liquidus temperatures of the copper smelting slag always increase with increasing ZnO concentration in the slag. The introduction of 4 wt% CaO, MgO or Al$_2$O$_3$ into the ZnO–"FeO"–SiO$_2$ slag significantly increases the liquidus temperature in the spinel primary phase field. It seems that the liquidus temperatures are more sensitive to the CaO and MgO concentrations than that of Al$_2$O$_3$.
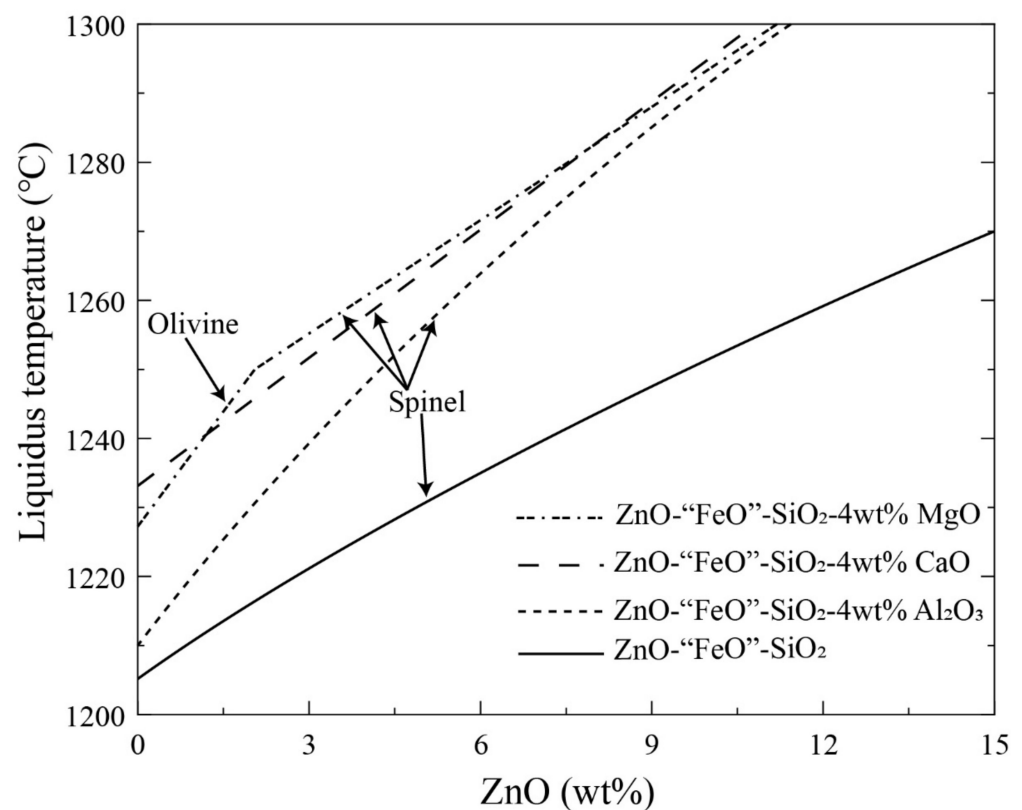

Figure 7. Effects of 4 wt% Al$_2$O$_3$, CaO or MgO on liquidus temperatures of the ZnO–"FeO"–SiO$_2$ slag at fixed FeO/SiO$_2$ = 1.9 (in mass) and Po$_2$ 10^{-8} atm. Reprinted with permission from ref. [33]. Copyright 2021 Elsevier.

An experimental technique was further developed to determine phase equilibria of the copper smelting slags under conditions closer to the smelting process. The phase equilibria in the systems "FeO"–SiO$_2$, "FeO"–SiO$_2$–CaO and "FeO"–SiO$_2$–CaO–MgO were experimentally investigated at fixed P(SO$_2$) = 0.3 and 0.6 atm and a fixed matte grade 72 wt% Cu [37–39]. Figure 8 shows the effects of 2 wt% CaO or MgO on the liquidus temperatures in the spinel primary phase field at fixed P(SO$_2$) = 0.3 atm with a fixed matte grade of 72 wt% Cu [38]. The predictions by FactSage 7.3 were also shown in the figure for comparison. It can be seen from the figure that, both the predictions and experimental results indicate that the liquidus temperatures decrease with increasing SiO$_2$ concentration in the spinel primary phase field. The presence of 2 wt% CaO or MgO significantly increases the liquidus temperatures. To keep a constant liquidus temperature, more SiO$_2$ flux is required which will increase the slag volume. FactSage 7.3 predicted much lower liquidus or less SiO$_2$ flux than the experimental results as no experimental data were reported in such complex conditions for FactSage optimisation.
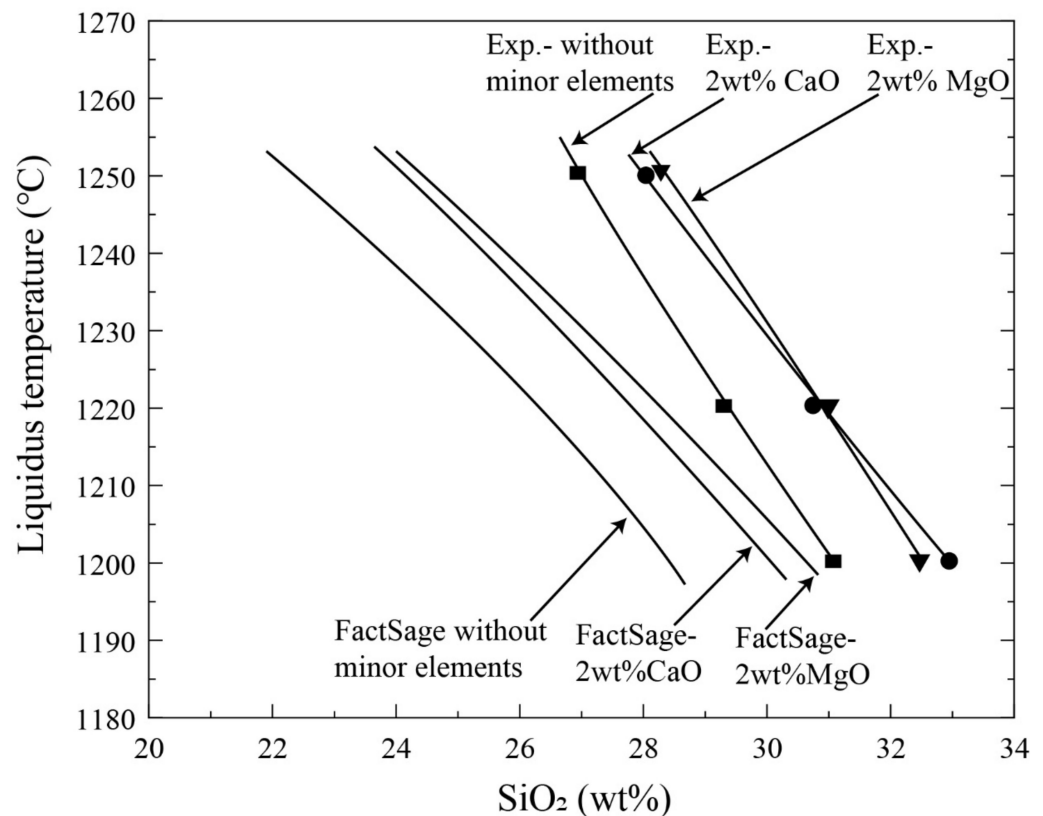
Figure 8. Effects of 2 wt% CaO or MgO on the liquidus temperatures in the spinel primary phase field at a fixed $P(SO_2) = 0.3$ atm and matte grade 72 wt% Cu, in comparison between experimental (symbols) and predicted (lines) results by FactSage 7.3. Reprinted with permission from ref. [38]. Copyright 2021 Elsevier.

With increased impurities in copper concentrates, control of the minor elements is an important issue in the copper smelting process. Based on the principle of Gibbs energy minimisation and the technological features of the BBS process, a multiphase equilibrium model SKS simulation software (SKSSIM) was developed [40,41]. Distributions of As, Bi, Sb, Pb and Zn as a function of matte grade can be calculated among slag, matte and gas. The calculated distributions in the BBS process were different from that in the Isasmelt and the flash smelting processes [42–44].

3.3. Fluid Dynamic Studies

The major difference between BBS and other bath smelting technologies is the direction of gas injection and gas pressure. High-pressure gas injected from different directions significantly influences stirring energy, surface waves, plume eye and splashing. Fluid dynamics of the molten bath is an important issue to understand the advanced performance of the BBS. Extensive studies were conducted on the fluid dynamic behaviours of the BBF using a water model and CFD (Computational Fluid Dynamic) simulation [45–68]. Mixing behaviour [45–51], surface wave [52,53], plume eye [54], bubble behaviour [55–58], fluctuating behaviour [59] were studied by water model to simulate the molten bath in BBF. Lance arrangement [60–62], gas–liquid multi-phase flows [63–65], flow and mixing behaviour [66] and multiphase interface behaviours [67,68] in the BBF were studied by the CFD method. A summary of the research on the fluid dynamic of the molten bath in BBF is presented in Table 4. Some examples are given in the following sections.

Table 4. Summary of the research on the fluid dynamic studies for the molten bath of BBF.

Reference	Research Method	Objects	Main Findings
Wang et al. [46,47]	Water model	Mixing behaviour	Effects of bath height, installation angles of nozzle and gas flow rate on velocity distribution
Shui et al. [48]	Water model	Mixing behaviour	Effects of gas flow rate and bath height on mixing time
Shui et al. [49]	Water model	Mixing behaviour	Effects of industry-adjustable variables on bath mixing time
Jiang et al. [50,51]	Water model	Mixing behaviour	Effect of horizontal distance between tuyeres, gas flow rate and bath height on mixing time
Shui et al. [52]	Water model	Surface wave	Effect of blowing angle, gas flow rate and bath height on mixing time on 1st asymmetric standing wave
Shui et al. [53]	Water model	Surface wave	Amplitude and frequency of surface longitudinal waves
Jiang et al. [54]	Water model	Plume eye	Effects of different operating parameters on the sizes of the plume eyes
Wang et al. [55,56]	Water model	Average diameter of bubbles	An empirical formula developed for average bubble diameter
Cheng et al. [57,58]	Water model	Copper matte attachment behaviour	Effects of bubble on the copper losses to the smelting slags
Luo et al. [59]	Water model	Fluctuation behaviour	Effects of diameter, inclination angle, gas flow rate and liquid surface on the violent level of liquid level.
Yan et al. [60]	CFD	Lance arrangement	An optimised lance arrangement (diameter, spacing, inclination)
Zhang et al. [61]	CFD	Tuyere structure parameters	An optimised tuyere arrangement (spacing, size, angle)
Guo et al. [62]	CFD	oxygen lances	An optimised oxygen lance layout
Zhang et al. [63]	CFD, Water model	Gas–liquid multi-phase flows	The effects of bubble parameters, gas holdup distribution, inlet pressure variations and the fluid level fluctuation on oxygen–copper matte flow
Tang et al. [64]	CFD	Gas–liquid phase interaction	Gas residence time and liquid copper matte splashing phenomena under varying gas flow rates
Li et al. [65]	CFD	Gas–liquid multiphase flow	The characteristics of each flow region in the furnace are obtained
Shao and Jiang [66]	CFD Water model	Flow and mixing behaviour	The effect of nozzle arrangement and gas flow rate on mixing time
Zhang et al. [21]	CFD	Bubble behaviour	The relation between mixing efficiency and bubble characteristics
Guo et al. [67]	CFD	Mechanism and multiphase interface behaviour	The capacity of BBS can be raised by reasonably controlling the potential value in different layers and regions
Guo et al. [68]	CFD	Optimisation of smelting process	Matte grade and slag type have deep effect on copper in slag

In a molten bath, the first step of the reactions is the melting of the concentrate particles and decomposition of the sulphides, such as FeS_2 and $CuFeS_2$. These sulphides are then oxidised to form FeS–Cu_2S matte and iron oxides (FeO, Fe_2O_3). The iron oxides generated by the reactions continuously react with SiO_2 to form slag which is insoluble to matte and floats on the top of the matte layer. On the other hand, the injected oxygen reacts with iron, copper and sulphur on the bottom of the bath to generate all heat to maintain the temperature of the molten bath. The mass and thermal transfer inside the molten bath significantly affect the reaction efficiency of the BBF. Cai et al. [69] did experiments

in a physical model of a bottom-blowing lead smelting furnace to find an optimal lance arrangement and configuration. An empiric calculation formula was concluded by normal hydraulic model test:

$$S/W = 26.224 \cdot (W/D_0)^{-0.629} \cdot (\mathrm{Fr}')^{0.122} \cdot (H/D)^{0.523} \tag{1}$$

where S is the effective stirring diameter of the oxygen lance, W is the space between oxygen lances, D_0 is the inner diameter of the export oxygen lance, Fr' is the modified Froude number, H is the depth of bath pool, D is the inner diameter of the furnace. In a late study, Shui et al. [48] defined effective stirring range D_e quantitatively and developed the 1st empiric equation to characterise the mixing behaviour of the copper BBF.

Figure 9 shows the mixing time as a function of distance from the lance at different depths of the bath [48]. In the water model experiments, 4 M KCl solution as a tracer of electric conductivity was added directly on the top of the gas injection lance. An electrode connected to a potentiostat was put in the required position to measure the electric conductivity of that location. The time to reach a stable electric conductivity was defined as "mixing time". It can be seen that within 220 mm the mixing time on the surface decreases slightly and then increases sharply with increasing the distance between the lance and electrode. However, D_e is different at different depths of the bath and increases with increasing the depth. When the horizontal distance from the lance is greater than D_e, the mixing time increases rapidly with increasing the distance. The maximum distance between two neighbour lances is the D_e on the surface to ensure the whole bath in the reaction zone can be efficiently stirred.
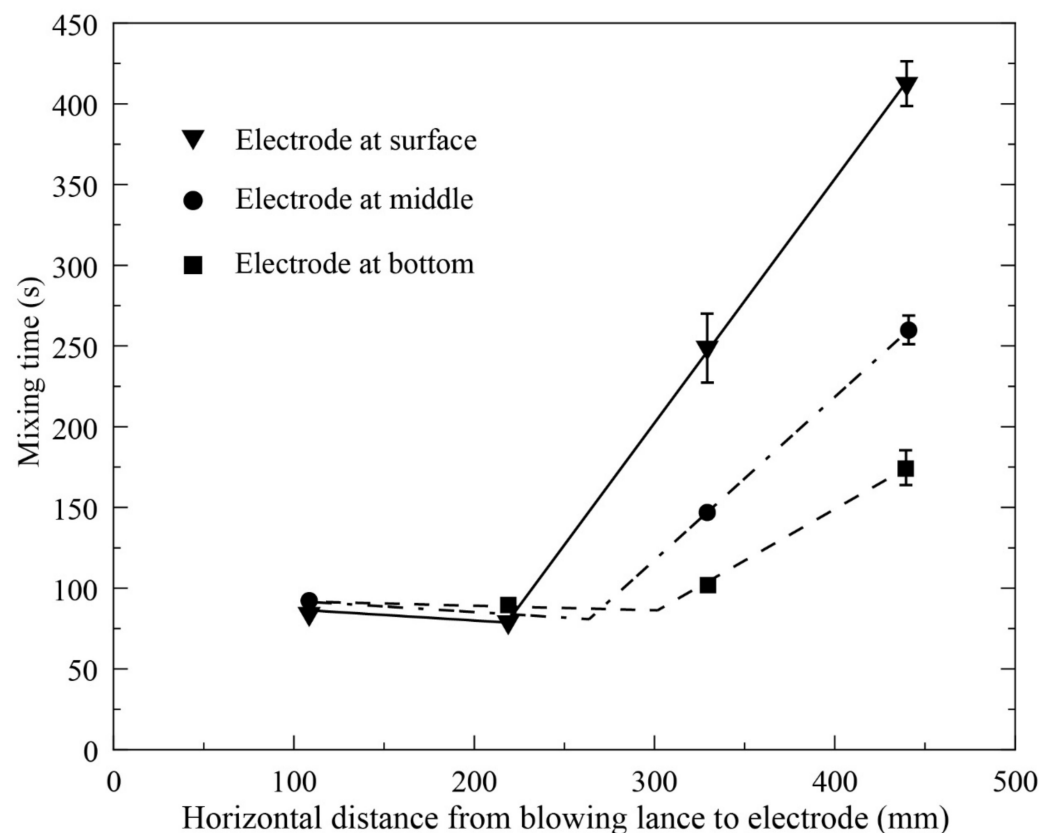

Figure 9. Mixing time vs. horizontal distance, at gas flow rate 150 mL/s, bath height 10 cm. Reprinted with permission from ref. [48]. Copyright 2021 Springer Nature.

The empiric equation to characterise the mixing behaviour of the copper BBF was obtained from the experimental measurements of the water model [48]

$$\tau = 37.5Q^{-0.39}h^{-1.08} \tag{2}$$

where τ is mixing time, Q is gas flow rate and h is bath height. Several important findings from this study can be directly applied to BBS:

1. The effective stirring range can be accurately determined for a single lance which is one of the important parameters to design the number of lances and distance between the lances. The optimum number and distance of the lances enable the bath to be efficiently mixed with minimum energy and gas consumption.

2. Within the effective stirring range, the mixing time is not sensitive to the vertical locations. However, the effective stirring range is smaller on the surface and mixing energy decreases much faster at the surface beyond the range. In copper BBF, many reactions occur on the surface of the bath as all solid materials are fed from the top. It is therefore important to ensure the surface area in the reaction zone is fully covered within the effective stirring area by proper arrangement of the lances.

3. Equation (2) is the first quantitative expression of the mixing time for copper BBF. Required injection gas flow rate and bath height can be calculated from this equation according to productivity.

In copper BBF operation, molten matte is covered by a thick slag layer. The fluid dynamic studies for a single layer bath are not enough to accurately describe the molten bath of the copper BBF. Jiang et al. [50] and Shui et al. [49] studied mixing behaviours of two-layer baths by using silicon oil and water to simulate slag and matte, respectively. It can be seen from Figure 10 that the changes in mixing time are not significant when the water thickness increases from 0.07 m to 0.09 m, but there is a sharp decrease when the water thickness exceeds 0.09 m. This indicates that a minimum matte height is required to generate enough stirring energy to mix the bath efficiently. In addition, it can be seen that the trends are similar at different gas flow rates.
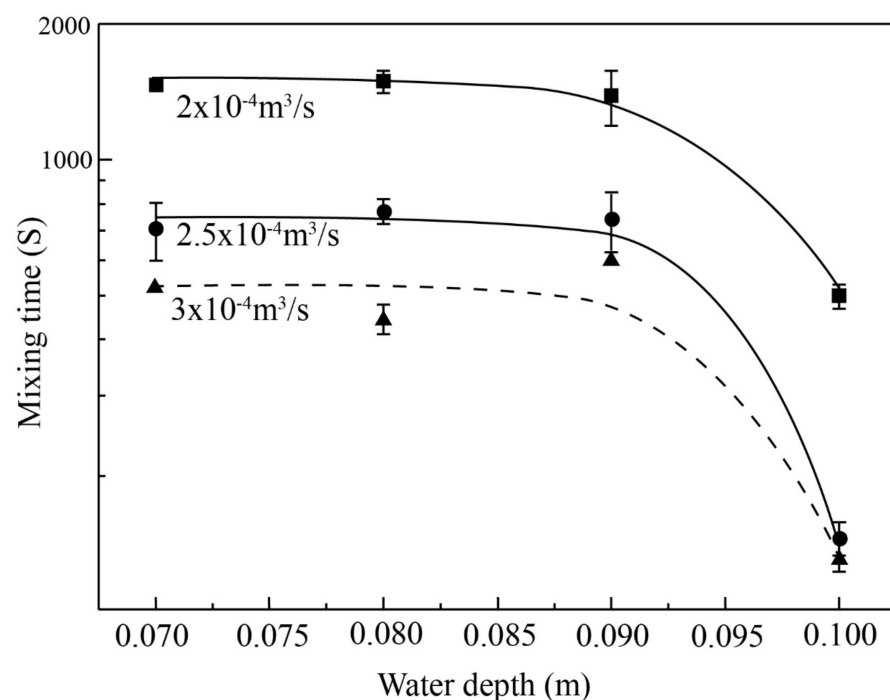

Figure 10. Effect of water height on mixing time at different gas flow rates, 0.03 m thick oil with viscosity 5×10^{-5} m^2/s on the top, symbols are experimental points. Reprinted with permission from ref. [49]. Copyright 2021 Springer Nature.

An empiric equation was also generated for a two-layer bath in copper BBF [49]. Four variables H, Q, h, ν_s were converted into SI units and correlated with the experimental mixing time in an overall multiple regression:

$$\tau = 7.31 \times 10^{-5} H^{-3.10} Q^{-2.29} h^{2.32} \nu_s{}^{0.27} \tag{3}$$

where τ is mixing time, Q is gas flow rate, H is water height, h is oil height and ν_s is oil viscosity.

The waves formed on the bath surface play important role in the BBF operations. Tapping of the viscous slag, corrosion of the refractory around the surface and settlement of the matte droplets in the slag are all associated with the bath waves. Simulation experiments were carried out to investigate the features of the waves formed on the bath surface of the BBF [52,53]. It was found that the ripples, the 1st asymmetric standing wave and the 1st symmetric standing wave can occur in the BBF bath. Empirical occurrence boundaries were determined from water model experiments. The amplitude of the 1st asymmetric standing wave was found to be much greater than the 1st symmetric standing wave and the ripples. The amplitudes increase with increasing bath height and flow rate but decrease with blowing angle. The frequency of the 1st asymmetric standing wave was found to increase with increasing bath height but be independent of gas flowrate and blowing angle. The dimensionless number We can be expressed as

$$We = \frac{\rho_L Q_g^2}{\sigma D^3} \tag{4}$$

where ρ_L is liquid density (kg/m^3), σ is the surface tension of the liquid (dyn/cm), D is container inner diameter (mm), Q_g is gas flowrate (mL/s).

Figure 11 shows the conditions for the occurrence of the 1st asymmetric standing waves [53]. The solid curves show the correlated boundaries while the points show the experimental results. It can be seen that, in general, the boundaries of different blowing angles are similar in shape. On the right side of the boundary, the 1st asymmetric standing wave is present, while on the left side only minor ripples occur.
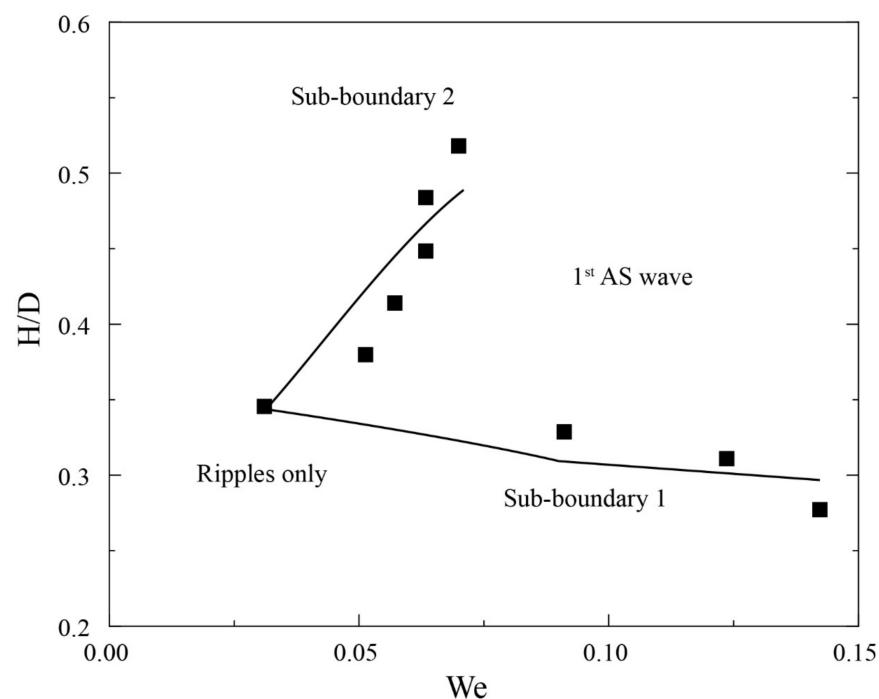

Figure 11. Occurrence condition of the 1st asymmetric standing wave at lance angle 7°, symbols are experimental points. Reprinted with permission from ref. [53]. Copyright 2021 Springer Nature.

During the Fangyuan BBF operation, it was observed from the feeding mouth that a plume eye was formed on the surface of the bath. The plume eye was initially observed and reported in the steelmaking process to describe the exposure of the lower liquid as the upper-level liquid was pushed away by the bottom injected gas. Through the water model experiments, it was found that the sizes of the plume eyes increase with increasing gas flow rate and lower liquid thickness, decrease with increasing upper liquid thickness [54]. Figure 12 shows the effects of gas flow rate and water height on the plume eye area at a fixed oil thickness.
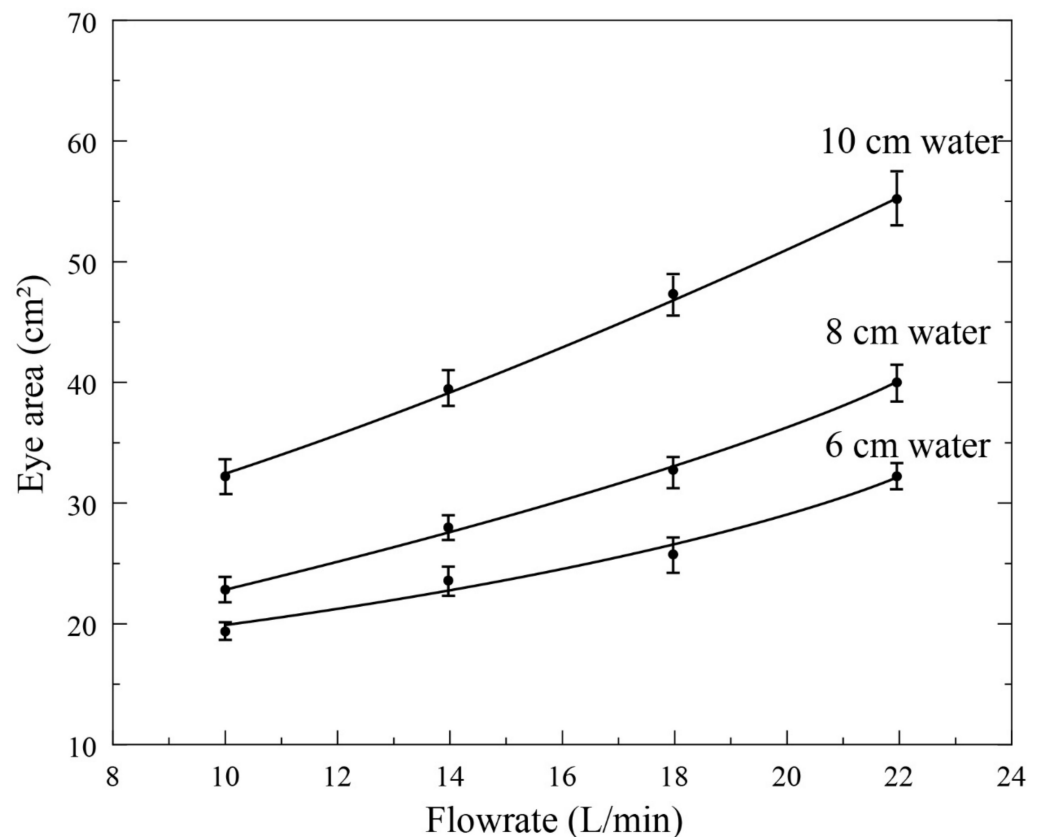

Figure 12. Effects of gas flow rate and water height on the plume eye area at a fixed oil thickness 4 cm. Reprinted with permission from ref. [54]. Copyright 2021 Springer Nature.

A modified model was developed in this study from the experimental data to predict the size of the plume eye [54]. Formation of the plume eye is important to understand the rapid reaction of the BBF. The presence of a plume eye below the feeding mouth means that the dropped copper concentrate (considered as low-grade matte) can enter and melt rapidly inside the matte layer where the oxygen partial pressure is relatively high. The formed iron and sulphur oxides in the matte raise to the slag layer.

4. Conclusions

Commercialised bottom-blowing copper smelting technology started in 2008. In less than 15 years this new technology has been developed rapidly to be the second-largest copper smelting technology. Development history and features of the new technology were reviewed from extensive publications. It is demonstrated that fundamental studies on slag chemistry and bath fluid dynamics have played an important role in supporting the development of this new technology. High-pressure gas injected from the bottom of the molten bath showed several advantages: (1.) generating a plume eye to allow the copper concentrate to react with matte directly; (2.) the surface waves assist in the tapping of the viscus slag so that low-temperature operation to produce high-grade matte with

high Fe/SiO$_2$ slag is possible; (3.) strong stirring energy to enable fast reactions in the molten bath resulting in high capacity and low-copper in the slag; (4.) high efficiency of oxygen utilization and heat absorption. The flexibility of the BBS on feeding materials and productivity is expected to not only increase its application in the copper industry to treat more complicated concentrates but also to enable the exploration of more applications of this technique in other high-temperature processes.

Author Contributions: Conceptualization, B.Z.; resources, B.Z.; data curation, B.Z. and J.L.; writing—original draft preparation, B.Z.; writing—review and editing, B.Z.; All authors have read and agreed to the published version of the manuscript.

Conflicts of Interest: The authors declare no conflict of interest.

References

1. Schlesinger, M.; Sole, K.; Davenport, W.; Alvear, G. Chapter 5—Theory to practice: Pyrometallurgical industrial processes. In *Extractive Metallurgy of Copper*, 6th ed.; Elsevier: Oxford, UK, 2021; pp. 95–117. ISBN 9780128218754.
2. Gonzales, T.W.; Walters, G.; White, M. Comparison of Smelting Technologies. In Proceedings of the 58th Annual Conference of Metallurgists (COM) Hosting the 10th International Copper Conference 2019, Vancouver, BC, Canada, 18–21 August 2019; p. 602421.
3. Wang, J. Copper smelting: 2019 world copper smelting data. In Proceedings of the 58th Annual Conference of Metallurgists (COM) Hosting the 10th International Copper Conference 2019, Vancouver, BC, Canada, 18–21 August 2019; p. 592732.
4. Watt, J.; Kapusta, J.P.T. The 2019 copper smelting survey. In Proceedings of the 58th Annual Conference of Metallurgists (COM) Hosting the 10th International Copper Conference 2019, Vancouver, BC, Canada, 18–21 August 2019; p. 595947.
5. Cheng, L.; Wang, Z.; Jiang, J.; Huang, Q. The SKS copper smelting process in China. In *Volume VI-Smelting, Technology Development, Process Modelling and Fundamentals, Proceedings of Copper 99-Cobre International Conference, Phoenix, AZ, USA, 10–13 October 1999*; Diaz, C., Landolt, C., Utigard, T., Eds.; The Minerals, Metals, and Materials Society: Warrendale, PA, USA; pp. 83–91. ISBN 0873394356.
6. Liang, S. A review of oxygen bottom blowing process for copper smelting and converting. In Proceedings of the 9th International Copper Conference (Copper 2016), Kobe, Japan, 13–16 November 2016; pp. 1008–1014.
7. Zhao, B.; Cui, Z.; Wang, Z. A new copper smelting technology—Bottom blown oxygen furnace developed at Dongying Fangyuan Nonferrous Metals. In Proceedings of the 4th International Symposium on High-Temperature Metallurgical Processing, San Antonio, TX, USA, 3–7 March 2013; pp. 3–10.
8. Cui, Z.; Shen, B.; Wang, Z.; Li, W.; Bian, R. New process of copper smelting with oxygen enriched bottom blowing technology. *Nonferr. Met. Extr. Metall.* **2010**, *3*, 17–20. (In Chinese)
9. Chen, Z. The application of oxygen bottom-blown bath smelting of copper. *China Nonferr. Metall.* **2009**, *5*, 16–22. (In Chinese)
10. Qu, S.; Li, T.; Dong, Z.; Luan, H. Plant practice of and design discussion on oxygen enriched bottom blowing smelting. *Nonferr. Met. Extr. Metall.* **2012**, *3*, 10–13. (In Chinese) [CrossRef]
11. Du, X.; Zhao, G.; Wang, H. Industrial application of oxygen bottom-blowing copper smelting technology. *China Nonferr. Metall.* **2018**, *4*, 4–6. (In Chinese) [CrossRef]
12. Wang, H.; Yuan, J.; He, R.; Wang, X. Plant practice of copper oxygen enrichment bottom blowing smelting. *Nonferr. Met. Extr. Metall.* **2013**, *10*, 15–19. (In Chinese)
13. Su, G.L. Discussion on practice of "blowing oxygen at the end of the catch matte" smelting. *China Nonferr. Metall.* **2010**, *4*, 5–8. (In Chinese)
14. Yan, J. Recent operation of the oxygen bottom-blowing copper smelting and continuous copper converting technologies. In Proceedings of the 9th International Copper Conference (Copper 2016), Kobe, Japan, 13–16 November 2016; pp. 13–16.
15. He, S.; Li, D. Discussion on issues related to Shuikoushan Copper Smelting process. *China Nonferr. Metall.* **2005**, *34*, 19–22. (In Chinese)
16. He, S.; Li, D. SKS copper smelting process. *China Nonferr. Metall.* **2006**, *35*, 6–9. (In Chinese)
17. Liang, S.; Chen, Z. Application and development of oxygen enriched bottom-blowing copper smelting technology furnace. *Energy Sav. Nonferr. Metall.* **2013**, *4*, 16–19. (In Chinese)
18. Kapusta, J.P.T. Implementation of air liquid shrouded injector (ALSI) technology at the Thai copper industries smelter. In *2007 International Copper Conference: The Carlos Diaz Symposium On Pyrometallurgy, Toronto, ON, Canada, 25–30 August 2007*; Warner, A.E.M., Newman, C.J., Vahed, A., George, D.B., Mackey, P.J., Warczok, A., Eds.; Canadian Institute of Mining, Metallurgy and Petroleum: Montreal, QC, Canada, 2007; Volume 3, pp. 483–500. ISBN 1-894475-73-9.

19. Kapusta, J.P.T.; Larouche, F.; Palumbo, E. Adoption of high oxygen bottom blowing in copper matte smelting: Why is it taking so long? In *Proceedings of the Torstein Utigard Memorial Symposium, Toronto, Canada, 23–26 August 2015*; The Materials and Metallurgical Society of CIM: Montreal, QC, Canada, 2015; pp. 1–25.

20. Kapusta, J.P.T. Submerged gas jet penetration: A study of bubbling versus jetting and side versus bottom blowing in copper bath smelting. *JOM* **2017**, *69*, 970–979. [CrossRef]

21. Coursol, P.; Mackey, P.J.; Kapusta, J.P.T.; Cardona Valencia, N. Energy consumption in copper smelting: A new Asian horse in the race. *JOM* **2015**, *67*, 1066–1074. [CrossRef]

22. Kapusta, J.P.T. Gas jet penetration, smelting intensity, and oxygen efficiency in side blowing versus bottom blowing. In Proceedings of the 9th International Copper Conference (Copper 2016), Kobe, Japan, 13–16 November 2016; pp. 1282–1305.

23. Kapusta, J.P.T.; Lee, R.G.H. The Savard-Lee shrouded injector: A review of its adoption and adaptation from ferrous to non-ferrous pyrometallurgy. In Proceedings of the 6th International Copper Conference (Copper 2013), Santiago, Chile, 1–4 October 2013; pp. 1115–1151.

24. Chen, M.; Cui, Z.; Wei, C.; Zhao, B. Degradation mechanisms of refractories in a bottom blown copper smelting furnace. In Proceedings of the 9th International Symposium on High-Temperature Metallurgical Processing, Phoenix, AZ, USA, 11–15 March 2018; pp. 149–157.

25. Chen, M.; Jiang, Y.; Cui, Z.; Wei, C.; Zhao, B. Chemical degradation mechanisms of magnesia–chromite refractories in the copper smelting furnace. *JOM* **2018**, *70*, 2443–2448. [CrossRef]

26. Chen, M.; Zhao, B. Investigation of the accretions in the bottom blown copper smelting furnace. In Proceedings of the 9th International Copper Conference (Copper 2016), Kobe, Japan, 13–16 November 2016; pp. 1184–1194.

27. Xu, L.; Chen, M.; Wang, N.; Gao, S. Chemical wear mechanism of magnesia-chromite refractory for an oxygen bottom-blown copper-smelting furnace: A post-mortem analysis. *Ceram. Int.* **2021**, *47*, 2908–2915. [CrossRef]

28. Chen, M.; Cui, Z.; Zhao, B. Slag Chemistry of Bottom Blown Copper Smelting Furnace at Dongying Fangyuan. In Proceedings of the 6th International Symposium on High-Temperature Metallurgical Processing, Orlando, FL, USA, 15–19 March 2015; pp. 257–264.

29. Cui, Z.; Wang, Z.; Zhao, B. Features of the bottom blown oxygen copper smelting technology. In Proceedings of the 4th International Symposium on High-Temperature Metallurgical Processing, San Antonio, TX, USA, 3–7 March 2013; pp. 351–360.

30. Chen, M.; Zhao, B. Comparison of slag chemistry between Teniente converter and flash smelting furnace. In Proceedings of the 9th International Copper Conference (Copper 2016), Kobe, Japan, 13–16 November 2016; pp. 967–975.

31. Bale, C.W.; Bélisle, E.; Chartrand, P.; Decterov, S.A.; Eriksson, G.; Gheribi, A.E.; Hack, K.; Jung, I.H.; Kang, Y.B.; Melançon, J.; et al. Reprint of: FactSage thermochemical software and databases, 2010–2016. *Calphad* **2016**, *55*, 1–19. [CrossRef]

32. Zhao, B.; Hayes, P.C.; Jak, E. Effects of CaO, Al_2O_3 and MgO on liquidus temperatures of copper smelting and converting slags under controlled oxygen partial pressures. *J. Min. Metall. Sect. B Metall.* **2013**, *49*, 153–159. [CrossRef]

33. Liu, H.; Cui, Z.; Chen, M.; Zhao, B. Phase equilibria in the ZnO-"FeO"-SiO_2-CaO system at P_{O_2} 10^{-8} atm. *Calphad* **2018**, *61*, 211–218. [CrossRef]

34. Liu, H.; Cui, Z.; Chen, M.; Zhao, B. Phase equilibria study of the ZnO-"FeO"-SiO_2-Al_2O_3 system at P_{O_2} 10^{-8} atm. *Metall. Mater. Trans. B* **2016**, *47*, 1113–1123. [CrossRef]

35. Liu, H.; Cui, Z.; Chen, M.; Zhao, B. Phase equilibria study of the ZnO-'FeO'-SiO_2-MgO system at P_{O_2} 10^{-8} atm. *Miner. Process. Extr. Metall.* **2018**, *127*, 242–249. [CrossRef]

36. Liu, H.; Cui, Z.; Chen, M.; Zhao, B. Phase equilibrium study of ZnO-"FeO"-SiO_2 system at fixed P_{O_2} 10^{-8} atm. *Metall. Mater. Trans. B* **2015**, *47*, 164–173. [CrossRef]

37. Chen, M.; Sun, Y.; Balladares, E.; Pizarro, C.; Zhao, B. Experimental studies of liquid/spinel/matte/gas equilibria in the Si-Fe-O-Cu-S system at controlled P(SO_2) 0.3 and 0.6 atm. *Calphad* **2019**, *66*, 101642. [CrossRef]

38. Sun, Y.; Chen, M.; Balladares, E.; Pizarro, C.; Contreras, L.; Zhao, B. Effect of MgO on the liquid/spinel/matte/gas equilibria in the Si–Fe–Mg–O–Cu–S system at controlled P(SO_2) 0.3 and 0.6 atm. *Calphad* **2020**, *70*, 101803. [CrossRef]

39. Sun, Y.; Chen, M.; Balladares, E.; Pizarro, C.; Contreras, L.; Zhao, B. Effect of CaO on the liquid/spinel/matte/gas equilibria in the Si–Fe–O–Cu–S system at controlled P(SO_2) 0.3 and 0.6 atm. *Calphad* **2020**, *69*, 101751. [CrossRef]

40. Guo, X.; Wang, S.; Wang, Q.; Tian, Q. Development and application of oxygen bottom blowing copper smelting simulation software SKSSIM. *Nonferr. Met. Sci. Eng.* **2017**, *27*, 946–953. [CrossRef]

41. Wang, Q.; Guo, X.; Tian, Q.; Jiang, T.; Chen, M.; Zhao, B. Development and application of SKSSIM simulation software for the oxygen bottom blown copper smelting process. *Metals* **2017**, *7*, 431. [CrossRef]

42. Wang, Q.; Guo, X.; Tian, Q.; Chen, M.; Zhao, B. Reaction mechanism and distribution behavior of arsenic in the bottom blown copper smelting process. *Metals* **2017**, *7*, 302. [CrossRef]

43. Wang, Q.; Guo, X.; Tian, Q.; Jiang, T.; Chen, M.; Zhao, B.J. Effects of matte grade on the distribution of minor elements (Pb, Zn, As, Sb, and Bi) in the bottom blown copper smelting process. *Metals* **2017**, *7*, 502. [CrossRef]

44. Wang, Q.; Wang, Q.; Tian, Q.; Guo, X. Simulation study and industrial application of enhanced arsenic removal by regulating the proportion of concentrates in the SKS copper smelting process. *Processes* **2020**, *8*, 385. [CrossRef]

45. Song, K.; Jokilaakso, A. Transport phenomena in copper bath smelting and converting processes–A review of experimental and modeling studies. *Miner. Process. Extr. Metall. Rev.* **2020**, *42*, 107–121. [CrossRef]

46. Wang, D.; Liu, Y.; Zhang, Z.; Shao, P.; Zhang, T. Experimental study of bottom blown oxygen copper smelting process for water model. *AIP Conf. Proc.* **2013**, *1542*, 1304–1307. [CrossRef]

47. Wang, D.; Liu, Y.; Zhang, Z.; Zhang, T.; Li, X. PIV measurements on physical models of bottom blown oxygen copper smelting furnace. *Can. Metall. Q.* **2017**, *56*, 221–231. [CrossRef]

48. Shui, L.; Cui, Z.; Ma, X.; Rhamdhani, M.; Nguyen, A.; Zhao, B. Mixing phenomena in a bottom blown copper smelter: A water model study. *Metall. Mater. Trans. B* **2015**, *46*, 1218–1225. [CrossRef]

49. Shui, L.; Cui, Z.; Ma, X.; Jiang, X.; Chen, M.; Xiang, Y.; Zhao, B. A Water model study on mixing behavior of the two-layered bath in bottom blown copper smelting furnace. *JOM* **2018**, *70*, 2065–2070. [CrossRef]

50. Jiang, X.; Cui, Z.; Chen, M.; Zhao, B. Mixing behaviors in the horizontal bath smelting furnaces. *Metall. Mater. Trans. B* **2018**, *50*, 173–180. [CrossRef]

51. Ma, X.; Cui, Z.; Contreras, L.; Jiang, X.; Chen, M.; Zhao, B. Fluid dynamics studies of bottom-blown and side-blown copper smelting furnaces. In Proceedings of the 58th Annual Conference of Metallurgists (COM) Hosting the 10th International Copper Conference 2019, Vancouver, BC, Canada, 18–21 August 2019; pp. 1–8.

52. Shui, L.; Ma, X.; Cui, Z.; Zhao, B. An investigation of the behavior of the surficial longitudinal wave in a bottom-blown copper smelting furnace. *JOM* **2018**, *70*, 2119–2127. [CrossRef]

53. Shui, L.; Cui, Z.; Ma, X.; Rhamdhani, M.A.; Nguyen, A.V.; Zhao, B. Understanding of bath surface wave in bottom blown copper smelting furnace. *Metall. Mater. Trans. B* **2015**, *47*, 135–144. [CrossRef]

54. Jiang, X.; Cui, Z.; Chen, M.; Zhao, B. Study of Plume eye in the copper bottom blown smelting furnace. *Metall. Mater. Trans. B* **2019**, *50*, 782–789. [CrossRef]

55. Wang, D.; Liu, T.; Liu, Y.; Zhu, F. Water model study of bubble behavior in matter smelting process with oxygen bottom blowing. *J. Northeast. Univ. Nat. Sci.* **2013**, *34*, 1755–1758.

56. Wang, D.; Liu, Y.; Zhang, Z.; Shao, P.; Zhang, T. Dimensional analysis of average diameter of bubbles for bottom blown oxygen copper furnace. *Math. Probl. Eng.* **2016**, *2016*, 4170371. [CrossRef]

57. Cheng, X.; Cui, Z.; Contreras, L.; Chen, M.; Nguyen, A.; Zhao, B. Introduction of matte droplets in copper smelting slag. In Proceedings of the 8th International Symposium on High-Temperature Metallurgical Processing, San Diego, CA, USA, 26 February–2 March 2017; pp. 385–394.

58. Cheng, X.; Cui, Z.; Contreras, L.; Chen, M.; Nguyen, A.; Zhao, B. Matte entrainment by SO$_2$ bubbles in copper smelting Slag. *JOM* **2019**, *71*, 1897–1903. [CrossRef]

59. Luo, Q.; Yan, H.; Jin, J.; Huang, Z.; Gong, H.; Liu, L. Gold model experiment on fluctuation behavior of liquid level in setting zone of bottom-blowing furnace. *Nonferr. Met. Eng.* **2020**, *10*, 46–53. [CrossRef]

60. Yan, H.; Liu, F.; Zhang, Z.; Gao, Q.; Liu, L.; Cui, Z.; Shen, D. Influence of lance arrangement on bottom-blowing bath smelting process. *Chin. J. Nonferr. Met.* **2012**, *22*, 2393–2400. [CrossRef]

61. Zhang, Z.; Yan, H.; Liu, F.; Wang, J. Optimization analysis of lance structure parameters in oxygen enriched bottom-blown furnace. *Chin. J. Nonferr. Met.* **2013**, *23*, 1471–1478. [CrossRef]

62. Guo, X.; Yan, S.; Wang, Q.; Tian, Q. Layout optimization of oxygen lances of oxygen bottom blown furnace. *Chin. J. Nonferr. Met.* **2018**, *28*, 2450–2550. [CrossRef]

63. Zhang, Z.; Chen, Z.; Yan, H.; Liu, F.; Liu, L.; Cui, Z.; Shen, D. Numerical simulation of gas-liquid multi-phase flows in oxygen enriched bottom-blown furnace. *Chin. J. Nonferr. Met.* **2012**, *22*, 1826–1834. [CrossRef]

64. Tang, G.; Silaen, A.K.; Yan, H.; Cui, Z.; Wang, Z.; Wang, H.; Tang, K.; Zhou, P.; Zhou, C. CFD study of gas-liquid phase interaction inside a submerged lance smelting furnace for copper smelting. In Proceedings of the 8th International Symposium on High-Temperature Metallurgical Processing, San Diego, CA, USA, 26 February–2 March 2017; pp. 101–111.

65. Li, D.; Dong, Z.D.; Xin, Y.; Cheng, L.; Guo, T.; Li, B.; Li, P. Research of gas–liquid multiphase flow in oxygen-enriched bottom blowing copper smelting furnace. In Proceedings of the 11th International Symposium on High-Temperature Metallurgical Processing, San Diego, CA, USA, 23–27 February 2020; pp. 975–986.

66. Shao, P.; Jiang, L. Flow and mixing behavior in a new bottom blown copper smelting furnace. *Int. J. Mol. Sci.* **2019**, *20*, 5757. [CrossRef]

67. Guo, X.; Wang, Q.; Tian, Q.; Zhang, Y. Mechanism and multiphase interface behavior of copper sulfide concentrate smelting in oxygen-enriched bottom blowing furnace. *Nonferr. Met. Sci. Eng.* **2014**, *5*, 28–34. [CrossRef]

68. Guo, X.; Wang, Q.; Tian, Q.; Zhao, B. Performance analysis and optimization of oxygen bottom blowing copper smelting process. *Chin. J. Nonferr. Met.* **2016**, *26*, 689–698. [CrossRef]

69. Cai, C.; Liang, Y.; Qian, Z. A model study on the continuous leadmaking process with bottom oxygen injection. *Chin. J. Process. Eng.* **1985**, *4*, 113–121. (In Chinese)